Enthalpy and Heat Capacity Changes for Formation of an Oligomeric DNA Duplex: Interpretation in Terms of Coupled Processes of Formation and Association of Single-Stranded Helices†

Jill A. Holbrook,‡ Michael W. Capp,§ Ruth M. Saecker,§ and M. Thomas Record, Jr.*,‡,§

Departments of Biochemistry and Chemistry, University of Wisconsin−Madison, 433 Babcock Drive, Madison, Wisconsin 53706

Received January 7, 1999; Revised Manuscript Received March 15, 1999

ABSTRACT: The thermodynamics of self-assembly of a 14 base pair DNA double helix from complementary strands have been investigated by titration (ITC) and differential scanning (DSC) calorimetry, in conjunction with van't Hoff analysis of UV thermal scans of individual strands. These studies demonstrate that thermodynamic characterization of the temperature-dependent contributions of coupled conformational equilibria in the individual "denatured" strands and in the duplex is essential to understand the origins of duplex stability and to derive stability prediction schemes of general applicability. ITC studies of strand association at 293 K and 120 mM Na^+ yield an enthalpy change of -73 ± 2 kcal (mol of duplex)$^{-1}$. ITC studies between 282 and 312 K at 20, 50, and 120 mM Na^+ show that the enthalpy of duplex formation is only weakly salt concentration-dependent but is very strongly temperature-dependent, decreasing approximately linearly with increasing temperature with a heat capacity change (282−312 K) of -1.3 ± 0.1 kcal K^{-1} (mol of duplex)$^{-1}$. From DSC denaturation studies in 120 mM Na^+, we obtain an enthalpy of duplex formation of -120 ± 5 kcal (mol of duplex)$^{-1}$ and an estimate of the corresponding heat capacity change of -0.8 ± 0.4 kcal K^{-1} (mol of duplex)$^{-1}$ at the T_m of 339 K. van't Hoff analysis of UV thermal scans on the individual strands indicates that single helix formation is noncooperative with a temperature-independent enthalpy change of -5.5 ± 0.5 kcal at 120 mM Na^+. From these observed enthalpy and heat capacity changes, we obtain the corresponding thermodynamic quantities for two fundamental processes: (i) formation of single helices from disordered strands, involving only intrastrand (vertical) interactions between neighboring bases; and (ii) formation of double helices by association (docking) of single helical strands, involving interstrand (horizontal and vertical) interactions. At 293 K and 120 mM Na^+, we calculate that the enthalpy change for association of single helical strands is approximately -64 kcal (mol of duplex)$^{-1}$ as compared to -210 kcal (mol of duplex)$^{-1}$ calculated for duplex formation from completely unstructured single strands and to the experimental ITC value of -73 kcal (mol of duplex)$^{-1}$. The intrinsic heat capacity change for association of single helical strands to form the duplex is found to be small and *positive* [$\sim$0.1 kcal K^{-1} (mol of duplex)$^{-1}$], in agreement with the result of a surface area analysis, which also predicts an undetectably small heat capacity change for single helix formation.

Almost a half-century after the discovery of the structure of the DNA double helix, major questions remain regarding its thermodynamic origins of stability. The entropy of helix formation is unfavorable, and stability is enthalpic at all temperatures (cf. refs *1* and *2*): What are the contributions of nearest-neighbor "vertical" interactions (e.g., π system stacking, burial of polar and nonpolar surface) and "horizontal" interactions between complementary bases (e.g., hydrogen bonding, burial of polar surface) to the favorable enthalpy of double helix formation from the individual strands? How does the intramolecular structure in single-stranded DNA (e.g., hairpin helices formed by folding; single helices formed by stacking of neighboring bases) affect the thermodynamics of duplex formation? Is there a heat capacity change (ΔC^o_{obs})[1] associated with duplex formation, and how can it be interpreted? Quantitative answers to these questions should aid in obtaining a general predictive scheme for DNA and RNA duplex stability (e.g., *3*, *4*).

Experimental estimates of ΔC^o_{obs} of DNA and RNA duplex formation vary widely, ranging from zero to very significant values [-100 cal K^{-1} (mol of base pair)$^{-1}$] (cf. *1*, *5*−*13*, and references therein). The ability to predict duplex stability and nucleic acid structure quantitatively and accurately from sequence requires knowledge of ΔC^o_{obs} and hence

† This work is supported by NIH Grants GM34351 and GM23467 (M.T.R.) and by an NIH Molecular Biophysics Traineeship (J.A.H.).

* Corresponding author.
‡ Department of Biochemistry.
§ Department of Chemistry.

[1] Abbreviations: S1, single-stranded DNA of sequence 5′-GCGTCATACAGTGC-3′; S2, single-stranded DNA of sequence 5′-GCACTGTATGACGC-3′; ITC, isothermal titration calorimetry; DSC, differential scanning calorimetry; ΔC^o_{obs}, observed constant pressure heat capacity change; *n*, stoichiometric equivalence point; UV, ultraviolet spectroscopy; A_{260}, absorbance at 260 nm; *R*, gas constant; T_m, midpoint transition temperature.

10.1021/bi990043w CCC: $18.00
Published on Web 06/06/1999

requires the resolution of this apparent discrepancy. Most current nearest-neighbor schemes for predicting DNA duplex stability on the basis of oligomer (i.e. lower temperature) or polymer (higher temperature) thermal denaturation data have assumed that $\Delta C^{o}_{obs} = 0$ (cf. *4*, *14*−*16*). However, if ΔC^{o}_{obs} for duplex formation is on the order of −100 cal K^{-1} (mol of base pair)$^{-1}$, the enthalpy change in base pair formation becomes 1 kcal mol^{-1} more negative for every 10 K increase in temperature, an effect which is far outside of the experimental uncertainty in $\Delta H°$. Predictions of the $\Delta H°$ of formation of the various nearest-neighbor base pair interactions from oligomer- and polymer-based DNA prediction schemes currently differ by 0−2 kcal (mol of base pair)$^{-1}$ with an average discrepancy of approximately 1 kcal (mol of base pair)$^{-1}$, with the polymer (higher T_m) values being more exothermic (cf. *4*, *14*), as expected if heat capacity effects are significant.

A related issue in a thermodynamic analysis of duplex formation and in the development of semiempirical relationships between the sequence of oligomeric or polymeric DNA and thermal (T_m) or thermodynamic ($\Delta G°$) stability concerns the structures of the initial and final states. Most thermal denaturation studies on oligomers have assumed that melting could be analyzed as a two-state transition between an intact duplex and denatured single strands. However, melting studies of oligomeric DNA sequences are typically complicated by coupled equilibria involving the duplex, including pretransition fraying of base pairs at ends of otherwise helical molecules (and in some cases by formation of stable partially denatured states in the transition region), as well as by post-transition coupled equilibria involving the "denatured" state (disruption of residual intrastrand structure). Thermodynamic contributions of all these coupled equilibria change with temperature. Both pre-transition and post-transition processes must be considered in determining appropriate transition baselines and in interpreting the thermodynamic quantities for the transition obtained from a given baseline assignment. For example, differences in baseline assignments appear to be the origin of differences in thermodynamic quantities obtained from van't Hoff (UV) and calorimetric melting studies of both double helical and single helical nucleic acids (see Results). Differential melting studies on interior regions of polymeric DNA, while not affected by fraying, are nevertheless complicated by questions regarding the extent of ordered structure in the "denatured" state of an internal loop. Among the many studies of duplex stability, only a few have quantified the effects of these coupled equilibria. For example, the contribution of residual stacked structure in the denatured state to the heat capacity change and thermodynamics of denaturation of polyA−polyU was quantified calorimetrically by Filimonov and Privalov (*11*), and the contribution of intramolecular hairpin formation (or other low-temperature cooperative intramolecular processes) in the denatured state to the thermodynamics of formation of a 13 bp oligomer duplex was quantified by Vesnaver and Breslauer (*5*) by calorimetric and van't Hoff analysis.

In this study, we propose a novel separation of observed thermodynamic quantities for duplex formation into contributions from formation and association (docking) of single-stranded (stacked) helices. The process investigated is the formation of a short DNA duplex from two complementary 14 base pair oligomers. Isothermal titration calorimetry (ITC) and differential scanning calorimetry (DSC) are used to determine enthalpies of double helix formation and dissociation. DSC and van't Hoff (UV) analysis of thermal denaturation are used to quantify the enthalpic contributions to duplex formation of temperature-dependent coupled processes in the duplex (end-fraying) and in the unpaired strands (hairpin folding, single helix formation). As in the key studies cited above (*5*, *11*), we find that coupled processes make very significant contributions to the observed thermodynamics (ΔH^{o}_{obs}, ΔC^{o}_{obs}) of duplex formation. In particular, the temperature-dependent noncooperative equilibrium between single helical (stacked) and unstructured states of single-stranded DNA contributes very significantly to the observed ΔH^{o}_{obs} and ΔC^{o}_{obs} of duplex formation and duplex denaturation at **all** temperatures.

The proposed decomposition of the observed thermodynamics into contributions from individual processes involving well-defined initial and final states of the strands provides a basis for quantitative comparisons between structure (i.e., changes in surface area) and thermodynamics. Correlations of this type (especially involving ΔC^{o}_{obs}) have led to significant advances in understanding protein stability and protein−ligand interactions (cf. *17*−*25*) and have been initiated in discussing aspects of nucleic acid stability (*3*). In our study, contributions of changes in water-accessible nonpolar and polar surface to the heat capacity changes for the formation of single and double helices are calculated from structural models and compared with our experimental results. We also propose a framework for analysis of the enthalpy of duplex formation from single helical strands in terms of changes in vertical and horizontal noncovalent interactions (e.g., interstrand stacking, base-pairing, changes in water-accessible polar and nonpolar surface area). Extension of this thermodynamic analysis to oligomers of different sequence and composition should yield an understanding of the structural basis for the observed differences in contributions to thermal and thermodynamic stability of GC and AT base pairs in different nearest-neighbor contexts.

METHODS

Purification of Oligonucleotides. Complementary DNA oligonucleotides of sequence 5′-GCGTCATACAGTGC-3′ (abbreviated S1) and 5′-GCACTGTATGACGC-3′ (abbreviated S2) were synthesized in five tritylated 1 μmol quantities by Operon, Inc. Strand sequences were designed to minimize the number of purine-purine nearest-neighbors in each strand. To reduce end-fraying of the duplex, both ends were capped with two GC base pairs, as in an earlier study (*5*).

As synthesized, the purities of the oligomers were approximately 74% for the S1 strand and 67% for the S2 strand, as calculated from the HPLC areas of microinjections of oligomers. Both oligomers were purified by HPLC using a column packed with a styrene−divinylbenzene copolymer and a solvent system of TEAA buffer (0.1 M triethlyamine, pH adjusted to 6.8 with glacial acetic acid) and acetonitrile. A continuous solvent gradient from 100% TEAA/0% acetonitrile to 50% TEAA/50% acetonitrile was used to elute the oligonucleotides. In the first HPLC run, the trityl-on peak was collected. The collected fraction was dried, detritylated by incubating it in a solution of 80% acetic acid for 30 min,

and dried down again. The detritylated fraction was dissolved in TEAA, reinjected on the same column system, collected, dried down, and washed repeatedly with triple-filtered water. Analytical HPLC was performed on the purified, detritylated oligos, using a FAX ion exchange column and continuous gradient elution beginning with 25 mM Na_2HPO_4 (pH 6.0) buffer and ending with 25 mM Na_2HPO_4 (pH 6.0) buffer plus 1 M NaCl. By this assay, S1 was ≥96% pure and S2 was ≥94% pure.

Oligonucleotide Solutions. Concentrations of stock solutions of purified oligonucleotides were determined as follows. An aliquot of the stock was accurately diluted (approximately 500-fold) to a final concentration of ~4 μM strand in Tris-Mg^{2+} buffer [0.1 M Tris base (Aldrich), 3 mM $MgCl_2$, adjusted with HCl to pH 9.2 at 296 K] and degraded into nucleoside monophosphates (NMP) with phosphodiesterase I (Worthington) at 250 μg/mL. Phosphodiesterase I has a pH optimum between 9.8 and 10.4 and an absolute requirement for Mg^{2+} (*26*). Progress of the degradation was monitored by following A_{260} of the sample at 298 K until the absorbance increase was complete (~10 min, as judged by an additional 2 h incubation period). Concentrations of stock oligonucleotide solutions were calculated from these absorbance plateaus using published extinction coefficients of the individual nucleoside monophosphates (*27*). Concentrations obtained by this method were systematically higher [6.4% (S2), 7% (S1)] than those estimated from the absorbance of the intact single strands at 298 K, using tabulated nearest-neighbor extinction coefficients (*27*). [Extinction coefficients of our structured strands in Tris-Mg^{2+} buffer at 298 K, determined by comparison of absorbances before and after degradation, are 1.25×10^5 L (mol of strand)$^{-1}$ cm^{-1} for S1 and 1.24×10^5 L (mol of strand)$^{-1}$ cm^{-1} for S2, with an uncertainty of approximately 2%.]

Double-helical oligomers were formed at a concentration of 175 μM duplex by mixing the two single-stranded oligonucleotides in a heat block at 353 K for 1 min, and then allowing the solution to cool to room temperature at a rate of approximately 0.5 K/min.

Isothermal Titration Calorimetry. The standard buffers for ITC studies (and also DSC and UV melting experiments) contained 0.1 mM Na_2EDTA, 10 mM Na_2HPO_4 (pH adjusted to 7.3 with HCl) and had a Na^+ concentration of 20 mM. Two additional buffers with total Na^+ concentrations of 50 and 120 mM were made by adding the appropriate amount of NaCl. Sufficient quantities of ITC solutions were prepared to perform a set of at least one titration of S2 into S1, or vice versa, at three different temperatures.

Stock solutions of S1 and S2 strands for ITC studies were prepared in these buffers at the oligomer concentrations (2.5−50 μM) listed in Table 1. Solutions were not dialyzed in order to avoid loss of sample, which occurs for these short oligomers even using dialysis tubing of the smallest available pore size. Even without dialysis, enthalpies of ITC injections of each individual oligomer into buffer, of buffer into buffer, and of excess oligomer into a solution of duplex were all the same as water into water injections, within error, from which we conclude that effects of any solvent mismatching are negligible.

Titrations were carried out on an Omega ITC (MicroCal, Inc.) equipped with a Fisher Scientific Isotemp 1016D water bath. Experiments were performed over the ranges 282−313 K and 20−120 mM Na^+. For each titration, one oligomer (2.5−5 μM strand concentration) was loaded into the 1.4 mL sample cell, and the complementary oligomer (at 25−50 μM strand concentration) was loaded into the 250 μL injection syringe. The stirring rate of the injection syringe was 400 rpm, and samples were equilibrated thermally prior to beginning a titration until the baseline had leveled off and the rms noise was less than 0.015 μcal s^{-1}. A typical titration consisted of 21 injections of 10 μL each, with 3 min between injections. Data from individual titrations were fit by Origin for ITC, version 2.9, to obtain the enthalpy change ΔH°_{ITC}, the stoichiometry (n), and the equilibrium constant (K_{obs}) for strand association. Out of 40 titrations, 1 was an outlier by the Q-test (>90% c.i.) and was eliminated from subsequent data fitting. At the temperatures and salt concentrations investigated, values of K_{obs} for formation of our 14 base pair duplex are expected to exceed 10^8 M^{-1}, too large to determine at the strand concentrations investigated by ITC (*28*). [At 2.5−5 μM strand concentrations, calculated values of K_{obs} exceed 4×10^5 M^{-1} at T_m. Use of ITC enthalpies in conjunction with the van't Hoff equation predicts that K_{obs} must be at least 3 orders of magnitude larger (i.e., $> 4 \times 10^8$ M^{-1}) at the high-temperature end of the range examined by ITC at each salt concentration.]

UV Thermal Scans. Thermal denaturation experiments with individual 14-mer strands and with 14 bp duplex DNA were carried out on a Cary Model 1 Bio UV−visible spectrophotometer equipped with a Peltier heating/cooling accessory and a temperature probe. Experiments were performed at 260 nm in dual beam mode, with a slit width of 1.8 mm and a 1 cm path length. The sample compartment was purged with dry nitrogen during runs. Scans typically were initiated at 276 K and ended at 368 K, with data collected every 0.3−0.5 K. Data were exported to Excel 5.0 (Microsoft) and corrected for thermal expansion. Thermal scans on the individual strands were performed at several different strand concentrations (typically spanning the range from 1.8 to 14 μM) to confirm the absence of significant contributions from interstrand interactions. Thermal scans were also performed in duplicate on NMP mixtures obtained by degradation of S1 and S2 single-stranded oligonucleotides in the Tris-Mg^{2+} degradation buffer. As a control, UV thermal scans were also performed with intact S1 and S2 oligomers in this Tris-Mg^{2+} buffer.

Differential Scanning Calorimetry. Differential scanning calorimetry was performed on the individual single strands and on the duplex using a MicroCal MC-2 microcalorimeter equipped with a Haake F3 temperature-controlled water bath. All DSC samples were made up in 120 mM Na^+ buffer, and all samples were run against 120 mM Na^+ buffer in the reference cell. Buffer−buffer baselines were run in 120 mM Na^+. Scan conditions for all DSC experiments were also as follows: sample and reference cells were equilibrated for 1 h at 278 K prior to the start of each scan; the scan rate was 90 K h^{-1}; data were collected between 283 and 383 K; and sample and reference cells were placed under 25 psi dry N_2 during the run. Single-stranded (S1,S2) oligomers were studied by DSC at concentrations of 360 μM strand; these samples were not removed from the cell between runs. Two independent samples of 14 bp duplex were prepared at strand concentrations of 175 μM, and each sample was scanned twice. To increase the reproducibility of repeat DSC scans,

samples were removed from the DSC and annealed by slow cooling (~0.5 K min^{-1}) prior to rescanning.

Data were fit using Origin for DSC, version 2.9 (MicroCal). For both the duplex and the single strands, buffer−buffer scans were subtracted from each sample scan, a baseline was fit, and the resultant area was integrated to give the enthalpy change in the process. A range of baselines was fit to each sample scan in order to obtain estimates of uncertainty in the enthalpy of the transition. To estimate the heat capacity change for duplex denaturation, the baselines were extrapolated to the midpoint temperature (as judged by the half-area of the transition), and the difference between them was measured. The uncertainty in the heat capacity change was estimated as above by fitting a range of baselines to each sample scan.

Calculation of Enthalpies and Fractional Extents of Folding from DSC Data. Both the enthalpy of folding and the fractional extents of folding of S1 and S2 (θ_{S1}^{fold}, θ_{S2}^{fold}) as a function of temperature were calculated from DSC data as follows. Because DSC scans could not be initiated below 283 K, the low-temperature baseline (corresponding to the completely folded state) could not be determined experimentally. The transition temperature for unfolding was independently obtained from the maximum in the DSC curve. To obtain the enthalpy of unfolding, we assumed that the heat capacity change in unfolding was negligible, and therefore treated the transition as being symmetrical about its midpoint temperature. Data at 120 mM Na^+, where >90% of the unfolding transition is observable, are completely consistent with these assumptions (see below) and with an onset of unfolding at about 277 K at this salt concentration. Values of θ^{fold} as a function of temperature were calculated from the corresponding fractional enthalpy change. Enthalpies of unfolding at 20 and 50 mM Na^+ were assumed to be the same as at 120 mM Na^+. However, unfolding is shifted to lower temperature at lower salt concentration, as judged by the temperature derivative of UV thermal scans (see Results). Fractional enthalpy changes and values of θ^{fold} as a function of temperature at 20 and 50 mM Na^+ were calculated by assuming the shape of the DSC curve was independent of [salt] and using the reduction in T_m (−5 and −7 K for S1, and −3.5 and −7 K for S2, in 50 and 20 mM Na^+, respectively) to shift the DSC curve obtained in 120 mM Na^+ to lower temperature.

van't Hoff Analysis of Denaturation of Duplexes and Single Helical Strands. van't Hoff enthalpies of duplex denaturation at each salt concentration (20, 50, 120 mM Na^+) were calculated from UV thermal scans by fitting linear sloping baselines to the pre-transitional (fraying) and post-transitional (residual single helix denaturation) regions, and using these baselines to calculate the fraction of double helical oligomers remaining (θ^{dh}) as a function of temperature. Then, for the process of duplex denaturation (dhd; S1·S2 ⇄ S1 + S2):

$$K^{dhd} = \frac{(1 - \theta^{dh})^2}{\theta^{dh}} C_{tot} \quad (1)$$

where C_{tot} is the total molar concentration of either S1 or S2 strand. At each salt concentration, the van't Hoff enthalpy of duplex denaturation was obtained from the derivative of ln K^{dhd} with respect to reciprocal absolute temperature, using data in the range $0.1 \leq \theta^{dh} \leq 0.9$:

$$\Delta H_{vH}^{dhd} = -R(\partial \ln K^{dhd}/\partial T^{-1}) \quad (2)$$

Fractional extents of formation of single-stranded helix in S1(θ_{S1}^{sh}) and in S2 (θ_{S2}^{sh}) as a function of temperature, T, were calculated directly from UV thermal scans of the individual strands at temperatures above the range of the unfolding transition. In this calculation, the baseline absorbances of the hydrolyzed NMP mixtures at T [$A_{260}^{NMP}(T)$] were used as the absorbances of the fully denatured (unstructured) state of the strands, and the extrapolated absorbances of the strands at 263 K [A_{260}(263 K)] were used as the baseline absorbances of the fully structured single-helical stacked state. Justifications for these baselines are considered in subsequent sections. On this basis, for the S1 strand:

$$\theta_{S1}^{sh}(T) = [A_{260}^{NMP}(T) - A_{260}^{S1}(T)]/[A_{260}^{NMP}(T) - A_{260}^{S1}(263\ K)] \quad (3)$$

To obtain an enthalpy of single helix formation from the UV thermal scans of each individual strand at each salt concentration, equilibrium constants K^{shf} for this process in each strand were calculated as a function of temperature assuming a two-state model. For S1:

$$K_{S1}^{shf} \equiv \frac{\theta_{S1}^{sh}}{1 - \theta_{S1}^{sh}} \quad (4)$$

For each strand at each salt concentration, values of ln K^{shf} were calculated from absorbance data in the range from 320 to 370 K ($0.4 \leq \theta^{sh} \leq 0.7$), spanning the apparent midpoint temperature of single helix denaturation (~350−360 K) but excluding the low-temperature range of the unfolding transition. The van't Hoff enthalpy of single helix formation was obtained as above from the derivative of ln K^{shf} with respect to reciprocal absolute temperature (cf. eq 2).

Surface Area Calculations. Double helical (B-form) DNA with the S1·S2 sequence and the corresponding single-helical strands of S1 and S2 were built using Insight II (Biosym Technologies) on an Octane workstation (Silicon Graphics), assuming that the conformations of the S1 and S2 single helices are the same as the conformations of these strands in the double helix. The disordered state of individual DNA strands was modeled using SYBYL (Tripos, Inc.). Single strands were built according to base composition using the "no conformation" assembly mode. In this "extended" model of the denatured state, alternate bases are flipped out from the sugar−phosphate backbone and rotated to varying extents, effectively eliminating all base−base interactions. Water-accessible surface areas of these DNA structures were calculated using a modified version of ANAREA (*29*; C. Bingman, personal communication), using a probe radius of 1.4 Å and van der Waals radii set I from Livingstone et al. (*30*). Estimates of the overlap of molecular surface of bases in forming single helical and duplex structures were obtained using the same van der Waals radii and a probe radius of 0.1 Å.

RESULTS

Thermodynamics of Duplex Formation and Denaturation. (a) Isothermal Titration Calorimetric Studies of Duplex

Table 1: ITC Determinations of the Enthalpy of S1·S2 Duplex Formation

expt	[Na^+] (mM)	T (K)	[S1] (μM)	[S2] (μM)	n	ΔH^o_{ITC} (kcal mol^{-1})
1	120	282.4	2.48	25.4	0.99	-61.0 ± 0.6
2		285.7	25.4	2.48	0.91	-65.6 ± 0.7
3		281.4	4.98	50.4	1.03	-58.5 ± 0.3
4		282.2	50.8	4.98	1.05	-62.5 ± 0.3
5		292.8	2.48	25.4	1.00	-70.6 ± 0.9
6		292.7	25.4	2.48	0.89	-74.5 ± 0.4
7		292.7	4.98	50.8	1.01	-71.4 ± 0.3
8		292.8	50.8	4.98	0.93	-74.4 ± 0.3
9		302.7	2.48	25.4	1.02	-83.8 ± 0.6
10		302.5	25.4	2.48	0.91	-90.3 ± 0.6
11		302.3	4.98	50.8	1.04	-83.3 ± 0.8
12		302.5	50.8	4.98	0.93	-87.7 ± 0.3
13		312.3	2.48	25.4	0.98	-95.5 ± 0.8
14		312.0	25.4	2.48	0.91	-100.8 ± 0.7
15		312.5	4.98	50.8	1.09	-93.1 ± 0.4
16		312.4	50.8	4.98	0.93	-102.5 ± 0.9
17	50	292.7	2.48	25.4	1.03	-72.0 ± 0.5
18		292.5	25.4	2.48	0.96	-71.4 ± 0.8
19		292.5	2.48	25.4	1.00	-73.3 ± 0.5
20		293.0	25.4	2.48	0.92	-73.8 ± 0.5
21		292.7	4.36	38.1	1.03	-74.0 ± 0.3
22		292.8	38.1	4.36	0.94	-76.0 ± 0.3
23		302.6	2.48	25.4	0.93	-92.9 ± 0.8
24		302.7	25.4	2.48	0.93	-88.6 ± 0.8
25		302.3	4.36	38.1	1.00	-88.3 ± 0.3
26		302.4	38.1	4.36	0.94	-90.2 ± 0.6
27		311.6	2.48	25.4	0.93	-104.0 ± 1.0
28		311.9	25.4	2.48	0.93	-102.5 ± 0.7
29		311.8	2.48	25.4	0.84	-105.4 ± 0.8
30		312.0	25.4	2.48	0.90	-99.7 ± 0.6
31		312.3	38.1	4.36	0.94	-99.6 ± 0.8
32	20	292.8	2.48	25.4	0.89	-71.4 ± 0.9
33		292.6	25.4	2.48	0.99	-83.8 ± 0.8
34		292.8	3.73	38.1	0.92	-78.2 ± 0.3
35		292.9	38.1	3.73	0.85	-78.4 ± 0.6
36		302.4	2.48	25.4	0.99	-83.3 ± 0.8
37		302.4	25.4	2.48	0.98	-93.8 ± 0.8
38		302.3	3.73	38.1	0.96	-89.6 ± 0.5
39		302.3	38.1	3.73	0.80	-93.0 ± 0.5

Formation. Enthalpies of association of complementary S1 and S2 strands to form a 14 bp duplex were determined by ITC at 10 K intervals between 282 and 312 K in 120 mM Na^+, as well as between 293 and 312 K in 50 mM Na^+ and at 293 and 302 K in 20 mM Na^+. All conditions investigated are summarized in Table 1. Representative examples of ITC experiments at 292 K (expt 8) and 312 K (expt 16) in 120 mM Na^+ are depicted in Figure 1A,B, respectively. Upper panels display the heat detected per injection; lower panels show the integrated data and the fit from which ΔH^o_{ITC} and the relative stoichiometry n were determined. In Figure 1A, for a titration of S1 into S2 (5 μM) at 292.8 K, $\Delta H^o_{ITC} = -74.4 \pm 0.3$ kcal (mol of duplex)$^{-1}$, the stoichiometry n is approximately unity, and the equilibrium constant for strand association, K_{obs}, is too large to determine ($K_{obs} > 5 \times 10^8$ M^{-1}). Figure 1B displays an analogous titration of S1 into S2 (5 μM) at 312.4 K, for which $\Delta H^o_{ITC} = -102.5 \pm 0.9$ kcal and n again is near unity. Clearly the magnitude of the heat effect is much larger at the higher temperature, for this pair of experiments in which all other conditions are identical. Although the data can be fit to an equilibrium constant $K_{obs} = 5 \times 10^7$ M^{-1}, this equilibrium constant is determined from the final 5−10% of the titration, and hence is for a strand population in the cell which may be significantly enriched in shorter oligomer sequences, despite the high purity (≥95%) of the strands. We therefore consider this K_{obs} to be only a lower bound on the actual 14-mer association equilibrium constant, which is calculated to exceed 4×10^8 M^{-1} under these conditions (see Methods).

Comparison of panels A and B of Figure 1 indicates that ΔH^o_{ITC} decreases strongly with increasing temperature [$\Delta\Delta H^o_{ITC}/\Delta T \cong -1.4$ kcal K^{-1} (mol of duplex)$^{-1}$]. This large temperature dependence of ΔH^o_{ITC} is the primary characteristic of the ITC data in Table 1; ΔH^o_{ITC} exhibits no significant dependence on strand concentration in the 2-fold range of our experiments, and is only weakly dependent on salt concentration. Consequently all ΔH^o_{ITC} at 20−120 mM Na^+ are plotted vs temperature in Figure 2, which shows that ΔH^o_{ITC} decreases linearly with increasing temperature, from -61 ± 2 kcal at 282 K (120 mM Na^+) to -98 ± 4 kcal at 312 K (120 mM Na^+). The slope of the linear least-squares fit to all data in Figure 2 yields a large negative heat capacity change for duplex formation: $\Delta C^o_{ITC} = -1.3 \pm 0.1$ kcal K^{-1} (mol of duplex)$^{-1}$.

At constant temperature, a small effect of salt concentration on ΔH^o_{ITC} is detectable in the data of Table 1; comparisons of ΔH^o_{ITC} at 292, 302, and 312 K indicate that ΔH^o_{ITC} decreases by approximately 5% as the salt concentration is reduced from 120 to 20 mM Na^+. We attribute this to the effect of salt concentration on the stability of folded (hairpin) structures in the S1 and S2 strands, as discussed below; in the absence of this [salt]-dependent coupled process, enthalpies of helix formation would be expected to be relatively independent of salt concentration, because Coulombic effects of salt concentration on duplex stability are largely entropic in aqueous solution (*11*, *31*−*33*). No effect of salt concentration on the heat capacity change is detected; individual values of ΔC^o_{ITC} for titrations performed in 120, 50, and 20 mM Na^+ buffers are -1.2 ± 0.1, -1.5 ± 0.1, and -1.2 ± 0.2 kcal K^{-1} (mol of duplex)$^{-1}$, respectively. Therefore, within error, ΔC^o_{ITC} is not a function of salt concentration. DSC and UV thermal scans, reported below, indicate that the duplex formed in association experiments at 312 K is only slightly frayed (∼2% denatured). Fraying cannot be the origin of the large negative ΔC^o_{ITC}.

(b) Differential Scanning Calorimetric Studies of Duplex Denaturation. To obtain the enthalpy change for the interconversion of the duplex and individual strands at a higher temperature, DSC was performed on S1·S2 duplexes in 120 mM Na^+ buffer (Figure 3). The onset of denaturation is approximately 305 K; denaturation is complete at approximately 350 K, with a T_m of 338.6 ± 0.7 K (defined as the maximum in the DSC scan). The shape of the melting curve is asymmetric, with a broad shoulder at low temperature, which we attribute primarily to the enthalpy of fraying of the ends of the duplex, but which may also contain a minor contribution from less stable helices formed by the residual (≤5%) level of contaminating failure sequences. The overall enthalpy of the transition (ΔH^o_{DSC}), including the low-temperature region, is 120 ± 5 kcal (mol of duplex)$^{-1}$.

Since ΔH^o_{DSC} is significantly larger in magnitude than the ITC enthalpies of helix formation obtained at lower temperatures, the denaturation heat capacity change must remain

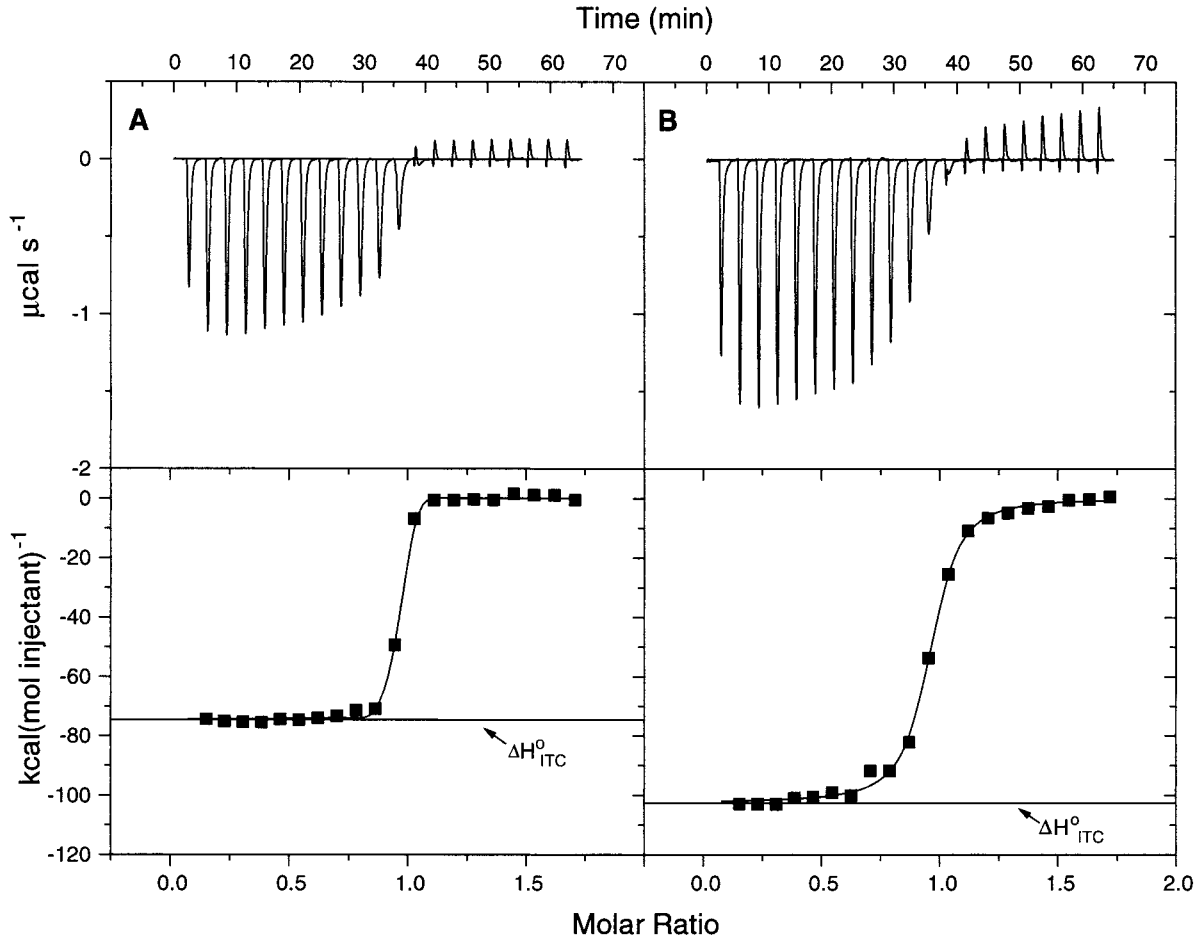

FIGURE 1: Comparison of ITC studies of duplex formation at 292.8 K (panel A) and 312.4 K (panel B). Conditions: 120 mM Na^+, [S2] = 4.98 μM (in ITC cell), [S1] = 50.8 μM (in injection syringe). The upper half of each figure shows the unnormalized heat effect (in μcal s^{-1}) detected after each of 21 successive 10 mL injections of S1 into S2. The lower half of each figure plots the corresponding integrated enthalpies of duplex formation, and the value of ΔH^o_{ITC} obtained from the Origin (Microcal) fit. Panel A: At 292.8 K (experiment 8 in Table 1), $\Delta H^o_{ITC} = -74.4 \pm 0.3$ kcal (mol of duplex)$^{-1}$, $n = 0.93$ and $K_{obs} \geq 5 \times 10^8$ M^{-1}. Panel B: At 312.4 K (experiment 16 in Table 1), $\Delta H^o_{ITC} = -102.5 \pm 0.9$ kcal (mol of duplex)$^{-1}$, $n = 0.93$, and $K_{obs} = 5 \times 10^7$ M^{-1}. Note that this value of K_{obs} is determined by the association behavior of the final 5−10% of the population of S2 strands.

large in magnitude at temperatures above 313 K. However, comparison of the ITC and DSC data indicates that ΔC^o_{obs} is temperature-dependent, decreasing in magnitude with increasing temperature. The difference between the high-temperature and low-temperature DSC baselines, extrapolated to 339 K, yields an estimate of the denaturation heat capacity change (ΔC^o_{DSC}) of 0.8 ± 0.4 kcal K^{-1} (mol of duplex)$^{-1}$, which is consistent with that estimated from the difference in enthalpies of helix formation at 313 and 339 K [~0.7 kcal K^{-1} (mol of duplex)$^{-1}$]. Linear extrapolation of ITC enthalpies to 339 K (cf. Figure 2) would predict a DSC denaturation enthalpy of 136 ± 4 kcal (mol of duplex)$^{-1}$, significantly larger in magnitude than the experimentally determined value of ΔH^o_{DSC} [120 ± 5 kcal (mol of duplex)$^{-1}$].

(c) UV Thermal Scans of Duplex Melting. UV thermal scans on duplex DNA samples (3.61 μM duplex) were performed in 20, 50, and 120 mM Na^+ buffer (Figure 4). These scans show the same overall trends as the DSC data (Figure 3). The onset of denaturation is detected at temperatures above 300 K as a gradual increase in A_{260}, characteristic of noncooperative fraying of the helix ends, which precedes the cooperative melting of the remainder of the double-stranded helix and is relatively independent of strand concentration and salt concentration. Midpoint transition temperatures, defined by the maximum in the derivative of the absorbance with respect to temperature, are 333.2 ± 0.5, 328.5 ± 0.3, and 321.0 ± 0.2 K in 120, 50, and 20 mM Na^+ buffer, respectively. The T_m at 120 mM Na^+ is approximately 6 K lower than that determined by DSC, a consequence of the much lower strand concentration in the UV thermal scan (3.6 mM) than in the DSC (175 mM).

Estimates of van't Hoff transition enthalpies at these salt concentrations from the temperature dependence of ln K^{dhd} (10−90% denaturation), using linear sloping baselines to calculate the fractional extent of denaturation as a function of temperature (see Methods), are approximately 100 ± 5 kcal. These values are approximately 15−20% smaller in magnitude than those estimated at these temperatures by interpolation of ITC and DSC data, consistent with the pre-transitional fraying of 1−2 bp at each end of these 14-mers at temperatures below the onset of the cooperative transition analyzed by the van't Hoff method. This pre-transition effect (~15−20%) is too large to be accounted for by the melting of any contaminating failure sequences (≤5%).

Thermal Transitions in the Individual S1 and S2 Strands. (a) UV Thermal Scans. To quantify the contributions of

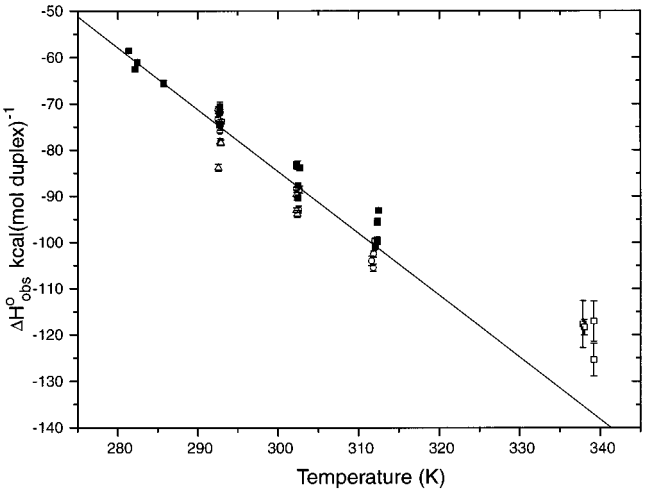

FIGURE 2: Values of ΔH^o_{ITC} versus temperature (K) at [Na^+] of 120 mM (■), 50 mM (○), and 20 mM (△) (cf. Table 1). A linear least-squares fit to the ΔH^o_{ITC} data gives the solid line with a slope (ΔC^o_{ITC}) of -1.3 ± 0.1 kcal K^{-1} (mol of duplex)$^{-1}$, the same within error as that determined for the most extensive (120 mM Na^+) data subset [-1.2 ± 0.1 kcal K^{-1} (mol of duplex)$^{-1}$]. Enthalpies of duplex formation at ~339 K and 120 mM Na^+ (□) obtained from DSC data (see Figure 3 below) deviate from the line defined by the ITC data.

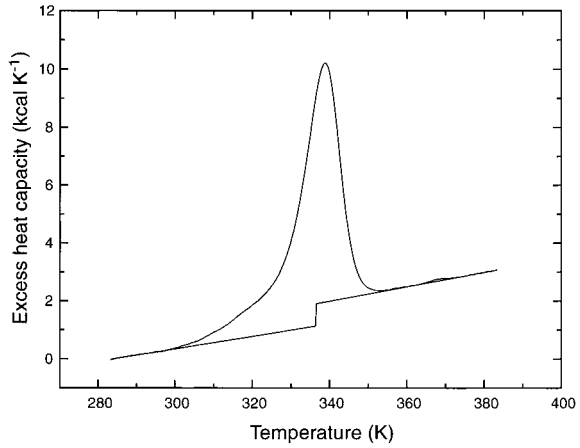

FIGURE 3: DSC of 175 μM duplex DNA in 120 mM Na^+ buffer. The excess heat capacity curve as a function of temperature is the average of four scans on two independent samples. From the baselines, $\Delta C^o_{obs} = 0.8 \pm 0.4$ kcal K^{-1} (mol of duplex)$^{-1}$ at $T_m = 338.6 \pm 0.7$ K. Integration of the excess heat capacity curve yields $\Delta H^o_{DSC} = 120 \pm 5$ kcal (mol of duplex)$^{-1}$.

temperature-dependent intramolecular folded and single helical (stacked) structure in the individual S1 and S2 strands to the observed thermodynamics of duplex formation, UV thermal scans of these strands were performed from 276 to 368 K at 20, 50, and 120 mM Na^+. Figure 5A,B shows these results, and compares them with the UV thermal scans of the corresponding NMP mixture and the duplex. Above 320 K, both S1 and S2 exhibit broad, monotonic salt concentration insensitive increases in absorbance with increasing temperature, which generally have been attributed to noncooperative unstacking of adjacent bases (e.g., *34*−*36*). (van't Hoff analysis of these data is presented under Discussion). In addition, a more cooperative low-temperature transition is observed between 280 and 320 K, which we attribute to unfolding of relatively unstable hairpins in each strand. (DSC analysis of the thermodynamics of unfolding is presented

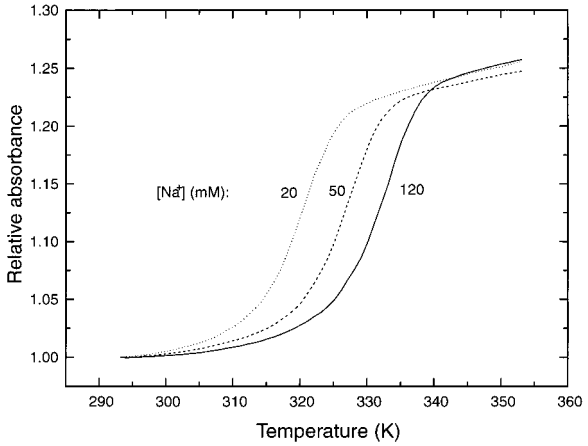

FIGURE 4: UV thermal scans of 14 bp S1·S2 duplexes at [Na^+] of 120 mM (—), 50 mM (- - -), and 20 mM (···). Absorbances at 260 nm are normalized to the absorbance at 293 K. Scans shown are the average of two determinations.

below.) The breadth of the unfolding transition in the single strands appears to be independent of [salt], and the midpoint (transition) temperature decreases with decreasing salt concentration. At 120, 50, and 20 mM Na^+, unfolding transition temperatures estimated from the maxima in dA_{260}/dT (cf. Figure 6, top) are 306 ± 2, 302 ± 2, and 300 ± 2 K for S1 and 302 ± 3, 300 ± 2, and 295 ± 3 K for S2. (These T_m values are independent of the choice of high- and low-temperature baseline within experimental uncertainty.) UV thermal scans at strand concentrations between 3.6 and 14 μM demonstrate that both the low- and high-temperature melting behavior of S1 and S2 are intramolecular.[2]

At temperatures above the unfolding transition (>320 K), Figure 5 demonstrates that the absorbances of both S1 and S2 increase approximately linearly with increasing temperature, with no apparent plateau at high temperature. This behavior is identical to that observed in the post-transition region of denaturation of the duplex, as shown in Figure 5. To compare the temperature-dependent UV absorbances of S1 and S2 with the end points expected for completely disordered, unstacked single strands, and thereby obtain high-temperature baselines for the disruption of single helix structure, S1 and S2 were degraded enzymatically into nucleoside monophosphates (NMP). At 368 K, the highest temperature investigated, values of A_{260} of the intact single strands are ~15% smaller than the absorbance of the NMP mixture, indicating that the strands are significantly ordered even at 368 K. UV scans of these solutions demonstrate the absorbance of the NMP mixture is relatively temperature-independent, decreasing by no more than about 2% over the experimentally accessible temperature range (Figure 5), in sharp contrast to the behavior of the individual S1 and S2 strands, for which the absorbance increases monotonically with increasing temperature with no evidence of a plateau even at the highest accessible temperature (368 K). We therefore conclude that the extents of intrastrand base−base interactions in both S1 and in S2 decrease gradually over

[2] Circular dichroism (CD) measurements on S1 as a function of temperature over the range from 220 to 300 nm (data not shown) showed the same transitions over the same temperature ranges as in the UV. No additional transitions were seen, and CD provided no additional information about the nature of the folded structure.

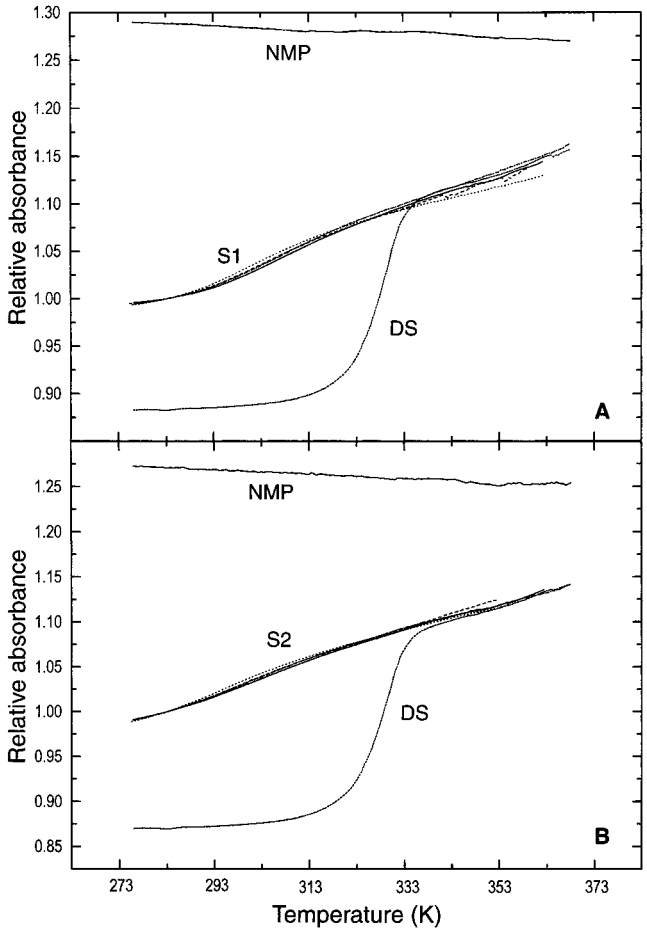

FIGURE 5: Temperature dependence of relative absorbances of individual strands, constituent nucleoside monophosphates (NMP), and duplex DNA, all corrected for thermal expansion. Panel A, S1; panel B, S2. Absorbances of the unpaired strands and NMP degradation products in each panel are expressed relative to those of the individual strand at 283 K. Scans of unpaired strands were performed at 120 mM [Na^+] (—), 50 mM Na^+ (- - -), and 20 mM Na^+ (•••), as well as in the Tris-Mg^{2+} degradation buffer (— • —), and are the averages of two determinations. The thermal scan of duplex DNA in Tris-Mg^{2+} buffer (— •• —) is given in each panel for comparison and is normalized to the high-temperature (368 K) absorbance of that strand. Thermal scans of nucleoside monophosphates in Tris-Mg^{2+} buffer are represented by (—).

the entire accessible temperature range (276−368 K) and are not eliminated even at 368 K.

(b) DSC Studies. Enthalpies of the cooperative low-temperature unfolding transitions of the individual strands were measured directly by DSC. As shown in Figure 6, the DSC scans in 120 mM Na^+ buffer show a significant heat absorption from 280 to 320 K for each strand, a range corresponding to that over which unfolding is observed by UV thermal scan. A direct comparison of the DSC scan and the temperature derivative of the absorbance data (Figure 6) shows an excellent correspondence between these two characterizations of unfolding. Unfolding midpoint temperatures at 120 mM Na^+ determined from the DSC scans (S1, 306 ± 1 K; S2, 301 ± 2 K, both at concentrations of 360 μM strand) agree within uncertainty with those determined from UV thermal scans at lower concentration and reported above. The lack of dependence of this transition temperature on strand concentration provides further evidence that the cooperatively melting structure is intramolecular.

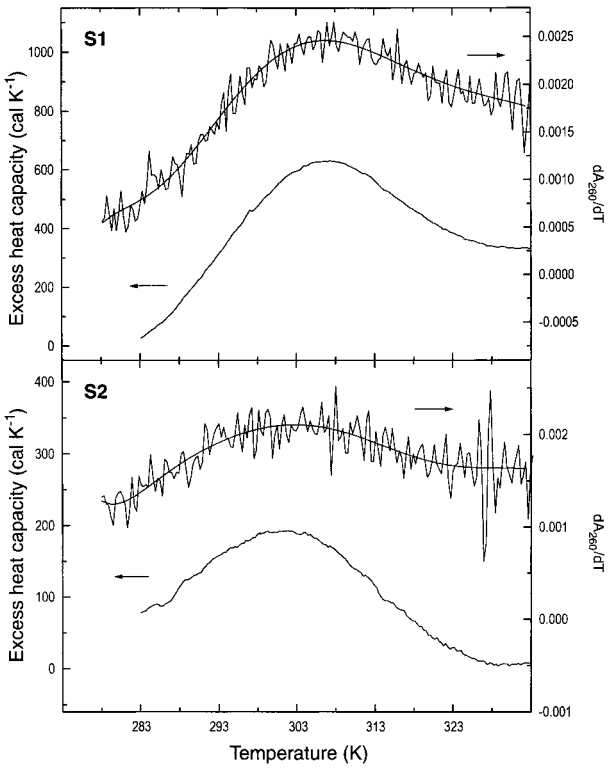

FIGURE 6: Comparison of DSC scans and derivative absorbance scans (dA_{260}/dT; data from Figure 5) for S1 and S2 in 120 mM Na^+ buffer. Top panel: Fit of the excess heat capacity data of S1 yields $\Delta H° = 14.0 \pm 0.7$ kcal (mol of strand)$^{-1}$ and $T_m = 305.8 \pm 1.0$ K. Bottom panel: For S2, $\Delta H° = 8.1 \pm 0.9$ kcal (mol of strand)$^{-1}$ and $T_m = 300.6 \pm 1.4$ K.

Unfortunately, the low-temperature (i.e., <283 K) baseline for each strand was not obtainable by DSC. However, both DSC and absorbance derivative profiles (Figure 7) suggest that the low-temperature baseline is attained in the vicinity of 280 K for both strands in 120 mM Na^+ buffer. Assigning a linear baseline to the unfolding transition, extending from 280 to 325 K, and assuming no heat capacity change in unfolding, we obtain DSC estimates of $\Delta H°_{unfold}$. For S1, $\Delta H°_{unfold} \cong 14.0 \pm 0.7$ kcal (mol of strand)$^{-1}$ and for S2, $\Delta H°_{unfold} \cong 8.1 \pm 0.9$ kcal (mol of strand)$^{-1}$ (see Methods). From the small magnitudes of $\Delta H°_{unfold}$, as well as from the dependence of T_m on [Na^+] observed in the UV thermal scans and the lack of a dependence of T_m on strand concentration, we infer that the low-temperature transition reflects unfolding of a hairpin involving the two terminal GC base pairs to form a relatively stacked single strand. The larger magnitude of the unfolding enthalpy for S1 may result from two possible wobble base pairs (GT and TG) which can form in the S1 strand but not in S2. [Shorter oligomers with two terminal GC base pairs have been shown to form more stable hairpins (*37*−*39*).]

ANALYSIS AND DISCUSSION

Coupled Processes Involving the Single Strands in Duplex Formation or Denaturation. ITC and DSC experiments demonstrate that the observed enthalpy of duplex formation becomes increasingly negative with increasing temperature, and that the correspondingly large negative heat capacity change also is temperature dependent, becoming less negative with increasing temperature. On the basis of previous work,

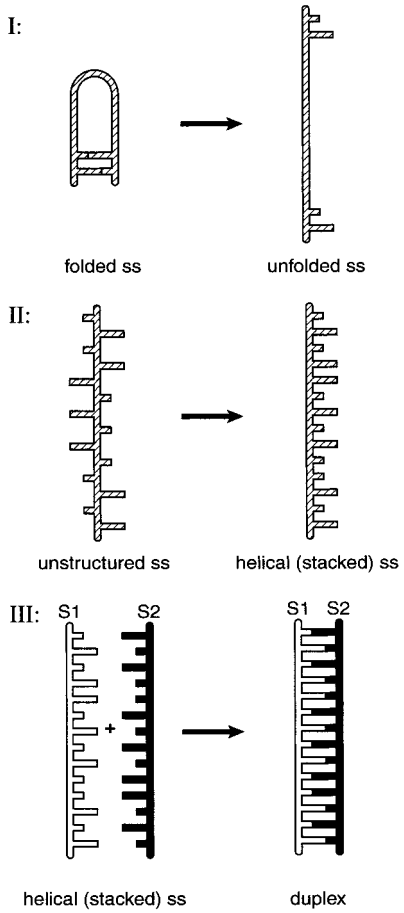

FIGURE 7: Schematic representation of processes I (unfolding of hairpin), II (single helix formation), and III (duplex formation by docking of stacked strands) which contribute to ΔH^{o}_{obs} of duplex formation at low temperature.

two possible origins of the large negative ΔC^{o}_{obs} of DNA helix formation (at low temperatures where fraying is insignificant) are (a) extensive removal of nonpolar surface from water not compensated by effects of removing polar surface from water (cf. *17*, *19*, *21*, *22*) and (b) temperature-dependent changes in the thermodynamic state of the single strands (e.g., *5*, *11*, *40*). Since the UV and DSC thermal scans of S1 and S2 indicate that the extents of single helix formation and folding in S1 and in S2 decrease significantly with increasing temperature in the range investigated, temperature-dependent changes in the thermodynamic state of both strands must be important determinants of ΔC^{o}_{obs}. In addition, and of even greater significance, these large differences in the structures of the single strands at different temperatures preclude direct interpretation of experimental values of ΔH^{o}_{ITC} and ΔH^{o}_{DSC} in terms of a single process.

To deconvolute the observed thermodynamics of duplex formation, we consider the following three intrinsic processes, as shown in Figure 7:

I. Unfolding: Cooperative intramolecular unfolding of hairpin structures in both S1 and S2 strands.

II. Single helix formation (shf): Noncooperative intramolecular assembly of a disordered strand into a single-strand helix (involving vertical intrastrand contributions from π stacking and removal of polar and nonpolar surface from water).

III. Association (docking) of single helices: Cooperative intermolecular assembly of single helical strands to form the double helix by interstrand interactions (both horizontal and additional vertical interactions). Horizontal contributions include base pairing and burial of polar and nonpolar surface; additional vertical contributions include interstrand π stacking and burial of polar and nonpolar surface.

In this deconvolution, the observed thermodynamics of duplex formation at a specified temperature are analyzed in terms of the cost of disrupting any existing folded structure in S1 or S2, the formation of vertical interactions between disordered bases in S1 and in S2 to yield fully ordered (helical) strands, and association of the ordered single strands. The association process (III) is thermodynamically equivalent to docking if the extent of intrastrand vertical interactions and single helical structure of each strand (as formed in process II) is not significantly changed in duplex formation (process III) by association of those ordered states. If this is not the case, the thermodynamics of process III include both docking and any conformational change occurring in either ordered strand. (Intertwining the single stranded helices would be a factor in the kinetics but not the thermodynamics of the docking or association process.) As an alternative to the above decomposition, the disordered state of the strands (no vertical interactions, no folding) may be used as the initial state, by combining rather than separating processes II and III above. However, since single helical structure in the individual strands is significant over the entire accessible temperature range (276−368 K), double helix formation from partially ordered strands in solution, especially at physiological temperatures, appears more closely related to process III than to the sum of processes II and III.

Given the above decomposition, the corresponding observed enthalpy of duplex formation (ΔH^{o}_{obs}) at temperature T can be related to the enthalpy of process III (ΔH^{o}_{dock}) at T by terms which represent the fractional contributions from unfolding and single helix formation in each individual strand:

$$\Delta H^{o}_{obs}(T) = \Delta H^{o}_{dock}(T) + [1 - \theta^{sh}_{S1}(T)]\Delta H^{o}_{shf,S1}(T) + [1 - \theta^{sh}_{S2}(T)]\Delta H^{o}_{shf,S2}(T) + [\theta^{fold}_{S1}(T)\Delta H^{o}_{unfold,S1}(T)] + [\theta^{fold}_{S2}(T)\Delta H^{o}_{unfold,S2}(T)] \quad (5)$$

where $\theta^{sh}(T)$ and $\theta^{fold}(T)$ are the fractional extents of single helix formation and of folding in each strand at temperature T. From eq 5, ΔH^{o}_{obs} differs from ΔH^{o}_{dock} by terms which involve not only the intrinsic enthalpies of ordering and folding but also the extent to which each occurs at a given T. For example, above 320 K, the strands are no longer folded ($\theta^{fold}_{S1} = \theta^{fold}_{S2} = 0$) and ΔH^{o}_{obs} is determined entirely by contributions from single helix formation and association as discussed below. The temperature dependence of the intrinsic enthalpies of unfolding, single helix formation, and double helix formation by docking of complementary single helical strands is determined by the corresponding heat capacity changes for each process. What are their magnitudes and signs? To address this question, we begin by examining the amounts of water-accessible surface area removed in single helix formation and docking.

Prediction of Intrinsic Heat Capacity Changes Involved in Single Helix Formation and Docking. Empirical relation-

Table 2: Changes in Nonpolar (ΔA_{np}) and Polar (ΔA_p) Water-Accessible Surface Areas for Processes of Formation and Docking of Single Helical Strands

process	$-\Delta A_{np}$ (Å^2)	$-\Delta A_{np}$ (Å^2)	f_p[a]
disordered S1 → helical S1	539	799	0.60
disordered S2 → helical S2	536	804	0.60
helical S1 + helical S2 → S1·S2 duplex	101	1259	0.93
disordered S1 + disordered S2 → S1·S2 duplex	1176	2862	0.71

[a] $f_p \equiv \Delta A_p/(\Delta A_p + \Delta A_{np})$.

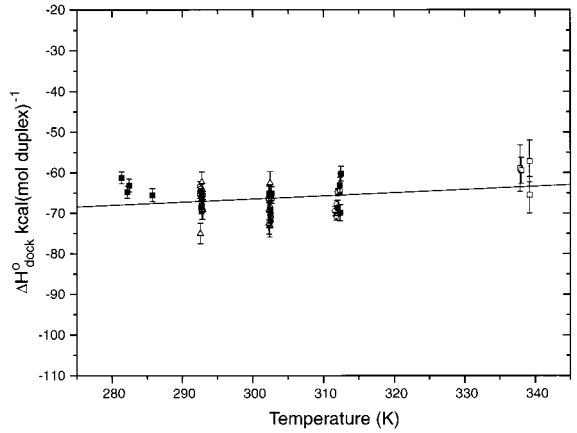

FIGURE 8: Values of ΔH^o_{dock} versus temperature (K) at 120 mM Na^+ (■), 50 mM Na^+ (○), and 20 mM (△) obtained by analysis of ITC and DSC (■) data (see eq 5 and Table 6). A linear least-squares fit of ΔH^o_{dock} as a function of temperature gives the solid line, with a slope of ~0.1 kcal K^{-1} (mol of duplex)$^{-1}$.

ships between changes in water-accessible surface area and ΔC^o_{obs} have been developed by a number of groups (cf. *19*−*22*). These relationships differ primarily in the choice of transfer process and in the compounds used to model the thermodynamic consequences of removing nonpolar or polar surface from water. From an analysis of the transfer of small hydrocarbons and amides from water to the pure liquid phase, the following expression quantitatively describes the ΔC^o_{obs} of transfer, protein folding, and protein−ligand interactions (*19*, *20*, *25*):

$$\Delta C^o_{obs} = (0.32 \pm 0.04)\Delta A_{np} - (0.14 \pm 0.04)\Delta A_p \quad (6)$$

(ΔA_{np} and ΔA_p represent changes, in Å^2,of nonpolar and polar water-accessible surface.) Since ΔA_{np} and ΔA_p make opposing contributions to ΔC^o_{obs}, an important result of eq 6 is that the magnitude of ΔC^o_{obs} depends fundamentally on the ratio of nonpolar to polar surface buried. As a consequence, large changes in nonpolar surface area do not necessarily give rise to large negative ΔC^o_{obs}, if offset by sufficiently large changes in polar surface area. This effect can be seen by rewriting eq 6 solely in terms of the fraction of the change in total surface area (ΔA_t) that results from ΔA_p ($f_p = \Delta A_p/\Delta A_t$):

$$(1/\Delta A_t)\Delta C^o_{obs} = (0.32 \pm 0.04) - (0.46 \pm 0.06)(f_p) \quad (7)$$

When f_p ~0.69, eq 7 predicts that ΔC^o_{obs} will be zero. The value of f_p for folding mid-sized globular proteins is approximately 0.4, for which case the burial of nonpolar surface dominates ΔC^o_{obs} (~75%) (*19*). What is the corresponding balance of nonpolar and polar contributions in helix formation?

Table 2 presents the values of ΔA_{np}, ΔA_p, and f_p for forming a single helical strand from a disordered single strand, for association of two helical strands to form the duplex, and for the overall process of forming the double helix from disordered single strands. Since the conformation of a completely "denatured" single strand is unknown, we used a model of an "extended" conformation of the single strand in which no vertical interactions exist between neighboring bases (see Methods). Single helix formation (process II; Figure 7) and association of single helices (process III) are both predicted to bury more polar surface than nonpolar surface: f_p is 0.60 for single helix formation and 0.71 for association (docking). As a consequence, the heat capacity change of converting a disordered 14-mer into a single helix (process II) is predicted by eq 6 to be negative but very small in magnitude ($\Delta C^o_{shf} = -60 \pm 40$ cal K^{-1} (mol strand)$^{-1}$ or -5 ± 3 cal K^{-1} (mol of nearest-neighbor stack)$^{-1}$], even though ~540 Å^2 of nonpolar surface is removed from water per strand in the process. In the association process (III), the burial of surface arises almost entirely from nitrogens and oxygens on the nucleic acid bases, and the heat capacity change is predicted to be positive in sign and again relatively small in magnitude [$\Delta C^o_{dock} = 0.14 \pm 0.1$ kcal K^{-1} (mol of duplex)$^{-1}$].

Since predicted intrinsic contributions to ΔC^o_{obs} from changes in nonpolar and polar surface in single helix formation (process II) and docking (process III) largely offset each other, we conclude that observed heat capacity changes in helix formation must arise primarily from temperature-dependent coupled processes in the unpaired strands. From an analysis of the DSC and UV thermal scan data on these strands, we obtain values of enthalpies of ordering the single strands and folding, and quantify the fractional extents of single helix formation and folding at a given temperature. These values, in combination with the observed values of ΔH^o_{ITC} or ΔH^o_{DSC}, allow us to extract a value of ΔH^o_{dock}. Changes in the states of the single strands with temperature are shown to give rise to the large negative temperature-dependent ΔC^o_{obs} of helix formation.

Cooperative Folding of Individual Strands. The DSC scans on the individual strands give a direct measurement of the heat required to disrupt the folded, cooperative intramolecular structure present at low temperatures (process I, above). The enthalpies of unfolding the single strands in 120 mM Na^+ are $\Delta H^o_{unfold,S1} \cong 14$ kcal (mol of strand)$^{-1}$ and $\Delta H^o_{unfold,S2} \cong 8$ kcal (mol of strand)$^{-1}$. Since the enthalpy of duplex formation is [salt]-independent, we assume that $\Delta H^o_{unfold,S1}$ and $\Delta H^o_{unfold,S2}$ are also [salt]-independent. Fractional extents of folding of S1 and S2 as a function of temperature, calculated as described under Methods, are listed in Table 4 below. Although we expect the folded structures in each strand are hairpins stabilized by base pairing interactions between the terminal GC pairs (cf. *37*−*39*), their three-dimensional structures are unknown. However, given the small predicted values of ΔC^o_{shf} and ΔC^o_{dock}, it is likely that the intrinsic heat capacity change associated with forming these intramolecular structures is small as well.

Table 3: Calculated Hypochromism of the Single Helical Strands (S1, S2) and the Duplex (S1·S2) Relative to Nucleoside Monophosphates (NMP)

	maximum hypochromism[a] (%)
NMP mixture	0
single helical S1	23.2 ± 0.1
single helical S2	22.8 ± 0.1
duplex S1·S2	31.6 ± 0.1

[a] Calculated from A_{260} extrapolated to 263 K (see text).

Table 4: Extents of Single Helix Formation and Folding in S1 and S2 Strands at 120 mM Na^+ [a,b]

T (K)	θ_{S1}^{sh}	θ_{S2}^{sh}	θ_{S1}^{fold}	θ_{S2}^{fold}
273	0.92	0.89	1.0	1.0
283	0.89	0.86	0.94	0.85
293	0.85	0.81	0.86	0.71
303	0.80	0.76	0.59	0.42
313	0.75	0.71	0.25	0.17
323	0.69	0.65	0.07	0.04
333	0.63	0.59	0.01	0
343	0.57	0.53	0	0
353	0.52	0.48	0	0
363	0.46	0.43	0	0
373	0.41	0.39	0	0

[a] Uncertainties do not exceed $\lesssim \pm 0.04$ for the specified choice of baselines. The fraction of single helix, θ^{sh}, is calculated from UV thermal scans as described under Methods. Values of θ^{sh} at temperatures below 320 K were calculated assuming the van't Hoff enthalpy is independent of temperature. The fraction of folded species, θ^{fold}, is calculated from DSC scans as described under Methods.

Noncooperative Single Helix Formation in the Individual Strands (Intrastrand Stacking). Disruption of single helical (stacked) structure in single-stranded polymeric [dA] (e.g., *34, 35*), poly[C] (*41*), and oligo- and poly[A] (e.g., *11, 34, 42, 43*) occurs over a very wide temperature range. Since the temperature ranges and breadths of the thermal transitions of the diribonucleotide ApA and poly[A] are similar under conditions where no strand association is involved, and van't Hoff enthalpies are comparable and relatively small ($\leq$10 kcal), the process of single helix formation by base stacking is thought to be noncooperative (*34*−*36*). UV and DSC thermal scans of oligomeric DNA sequences investigated here are broad as well: disruption of single helical structure in S1 and S2 takes place over a wide temperature range which appears to extend from below 273 K to above 373 K. In addition, folding transitions in S1 and S2 complicate the calorimetric study of denaturation of single helical structure study. Consequently, we were unable to quantify the enthalpy of denaturation of single helical (stacked) structure by DSC. Instead, we use van't Hoff analysis of absorbance data (Figure 5) characterizing single helix denaturation at temperatures greater than the temperature where the unfolding process ends (>320 K). This range of temperatures appears to include the T_m of this transition for both strands.

To obtain the enthalpy and fractional extent of single helix formation in the unpaired strands at a given temperature, low- and high-temperature UV baselines are needed, corresponding in the former case to the absorbance of the maximally stacked strand and in the latter to the completely unstacked strand. Assumptions are required in order to set these baselines, as has been the case in previous studies of stacking (e.g., *1, 11, 34, 36, 41*−*46*). For the high-temperature baseline, we propose use of the absorbance of the nucleoside monophosphate mixture obtained by degradation of each single strand, in which stacking interactions are completely abolished at the concentrations used (see Methods and Figure 5). Because the absorbances (cf. Figure 5) of the nucleoside monophosphate mixtures corresponding to the S1 and S2 strands are significantly higher and much less temperature dependent than those of the intact strands, even in the vicinity of 368 K, we conclude that the intact S1 and S2 strands retain significant stacked (single-helical) structure at 368 K. Although we cannot eliminate the formal possibility that the connectivity of unstacked bases in the unstructured strand might by itself reduce their absorbance, the qualitatively different temperature dependences of the intact strands and the nucleoside monophosphate mixtures argue strongly that the temperature-dependent absorbances of the intact strands in the vicinity of 368 K do not constitute the baseline behavior of completely unstructured strands.

For the low-temperature baseline, we use the (linearly) extrapolated absorbance at 263 K, corresponding to the temperature reported by Leng and Felsenfeld (*34*) for the beginning of poly[dA] unstacking. (Absorbances estimated in this manner for the fully structured states of S1 and S2 are 2−3% less than those observed at 283 K.) While experiments on strands which cannot fold are required to establish a more accurate low-temperature baseline, an independent argument for our choice is based on the hypochromism of the fully structured strands estimated from a linear extrapolation of absorbances to 263 K: 23.2% for S1 and 22.8% for S2 (Table 3). By comparison, the hypochromism of the S1·S2 duplex at this temperature is 31.6%. Hence, the hypochromism of the S1·S2 strands at 263 K is ~73% as large as the hypochromism of the duplex. We propose that the ~27% difference in hypochromism between the S1 or S2 strands and the duplex may be interpreted structurally in terms of the additional overlap of base rings (interstrand stacking) in the duplex relative to that in the stacked single strands. Indeed a calculation of the molecular surface of base ring atoms in a nucleotide, in the stacked single strands and in the duplex using a probe radius of 0.1 Å, reveals that ~27% of the total change in ring molecular surface occurs in docking the stacked S1 and S2 strands.

Using the absorbance of the depolymerized nucleoside monophosphates (NMP, Figure 5) for the high-temperature baseline and the extrapolated absorbance at 263 K for a low-temperature baseline (Table 3), the fractional extents of single-stranded (stacked) helical structure in S1 and in S2 were calculated from UV thermal scans (Figure 5). Table 4 quantifies these results; a significant degree of intrastrand stacked helix in S1 and S2 exists throughout the temperature range, decreasing gradually with increasing temperature. Two-state analyses of these data (from 320 to 370 K) yield very similar van't Hoff enthalpies of single helix formation for S1 and for S2 ($\Delta h_{shf,S1}^{vH} = -5.7 \pm 0.1$ kcal, $\Delta h_{shf,S2}^{vH} = -5.3 \pm 0.5$ kcal at 120 mM Na^+). Table 5 lists van't Hoff enthalpies and entropies as well as midpoint temperatures of single helix formation at 20, 50, and 120 mM Na^+. Assuming that single helix formation is noncooperative, we interpret the van't Hoff enthalpies in Table 5 as the enthalpies forming a nearest-neighbor vertical base−base interaction

Table 5: van't Hoff Enthalpies, Entropies, and Midpoint Temperatures (T_m) of Single Helix Formation

strand	[Na^+] (mM)	Δh^{vH}_{shf} (kcal)	Δs^{vH}_{shf} (eu)	T_m (K)
S1	20	-4.4 ± 0.1	-12.2 ± 0.1	363 ± 1
	50	-5.4 ± 0.1	-15.0 ± 0.1	358 ± 1
	120	-5.7 ± 0.1	-16.0 ± 0.1	356 ± 1
S2	20	-4.5 ± 0.7	-12.8 ± 2.1	353 ± 5
	50	-5.8 ± 0.1	-16.6 ± 0.2	347 ± 2
	120	-5.3 ± 0.5	-15.0 ± 1.3	351 ± 4

(containing contributions from π stacking and burial of polar and nonpolar surface).

Values of $\Delta h^{vH}_{shf,S1}$ and $\Delta h^{vH}_{shf,S2}$ given in Table 5 are similar to that (-7 kcal) obtained for poly[C] using DSC data with similar baseline assignments to ours (*41*), and are smaller in magnitude by 3−5 kcal than most other literature values for the van't Hoff enthalpy of single helix formation in homopolynucleotides (A, C), as estimated from absorbance measurements interpreted using baseline assignments which differ from ours (e.g., *35*, *36*, *41*, *42*, *44*, *45*). Values in Table 5 are somewhat larger (∼2−3 kcal) than the enthalpy of poly[A] single helix formation obtained from scanning calorimetric measurements, also with baseline assignments which differ from ours (*11*). We propose that the previous calorimetric and van't Hoff studies are both affected by assuming that the observed high-temperature (368 K) absorbance or DSC data correspond to a completely disordered single strand. Since the residual hypochromism of the strands at 368 K indicates to us that significant amounts of vertical base−base interactions remain at 368 K, assigning the 368 K state as the high-temperature baseline would cause values for the enthalpy of single helix formation from a van't Hoff analysis to be too large and cause calorimetric values to be too small.

Formation of the Duplex from Two Helical Unfolded Single Strands (Docking). Formation of a duplex from two complementary helical single strands involves forming hydrogen bonds between the bases, removing predominantly polar surface from water (Table 2), and forming additional $\pi-\pi$ interactions via interstrand stacking. We designate this process as docking (process III of Figure 7). (If association also involves a change in intrastrand vertical interactions, this contribution is combined with docking in process III). What is the enthalpy change for docking of fully stacked strands to form the duplex? How does it change with temperature? Assuming as a first approximation that ΔH^o_{fold} and Δh^{vH}_{shf} are relatively independent of temperature, we use eq 5 to obtain values of ΔH^o_{dock} as a function of T from experimental enthalpies of duplex formation (ΔH^o_{obs}) obtained from ITC and DSC experiments. Results are shown in Table 6 at 120 mM Na^+. From this calculation, we find that ΔH^o_{dock} is approximately -64 kcal (mol of duplex)$^{-1}$ at 283 K [-4.6 kcal (mol of base pair)$^{-1}$] and increases slightly to approximately -60 kcal (mol of duplex)$^{-1}$ at 339 K [-4.3 kcal (mol of base pair)$^{-1}$]. These small increases in ΔH^o_{dock} with temperature, shown in Figure 8, correspond to a small, *positive* intrinsic ΔC^o_{dock} of 0.1 kcal K^{-1} (mol of duplex)$^{-1}$, in good agreement with the value [0.14 ± 0.10 kcal K^{-1} (mol of duplex)$^{-1}$] calculated above from changes in polar and nonpolar surface area.

For the hypothetical process of forming a 14-mer duplex from two completely disordered single strands at 293 K, we calculate that ΔH^o_{obs} would be approximately -210 kcal (mol of duplex)$^{-1}$ ($\Delta H^o_{obs} = \Delta H^o_{dock} + 26\Delta h^{vH}_{shf}$), which corresponds to -15 kcal (mol of base pair)$^{-1}$. At 293 K, however, the experimental ITC value of ΔH^o_{obs} is -73 ± 2 kcal (mol of duplex)$^{-1}$, or -5.2 kcal (mol of base pair)$^{-1}$, and ΔH^o_{dock} is calculated to be -64 ± 4 kcal (mol of duplex)$^{-1}$, or -4.6 kcal (mol of base pair)$^{-1}$. Because vertical base−base interactions in each unpaired strand are extensive at physiological temperatures, helix formation at these temperatures is more similar to association of single helical strands than to association of unstructured (denatured) strands. A rough estimate of the contribution of interstrand vertical interactions to ΔH^o_{dock} can be obtained from the estimated increase in nearest-neighbor stacked surface (∼27%) upon docking of our single helical strands, together with the observed average enthalpy of single helix formation (-5.5 kcal). Vertical interactions assessed in this way could contribute approximately -40 kcal to ΔH^o_{dock}, or approximately two-thirds of its magnitude at 293 K. Experiments with other sequences and base compositions are required to assess the validity of this decomposition and to analyze the residual enthalpy of docking in terms of base pairing and other horizontal interactions.

Origin of the Observed Large Negative Heat Capacity Change of Duplex Formation: Enthalpically Significant Coupled Equilibria in the Single Strands. Table 6 presents the enthalpies of docking, folding, and single helix formation at 283, 313, and 339 K. Interestingly, at 283 K, estimated contributions from single helix formation and unfolding largely offset each other, and the enthalpy of docking is comparable to the observed enthalpy of helix formation. While the contribution from unfolding decreases to zero by 339 K, the requirement for formation of vertical base interactions (single helix formation) makes increasingly larger contributions to the observed enthalpy of helix formation with increasing temperature, because the initial state of the

Table 6: Dissection of Observed Enthalpy of Duplex Formation at 120 mM Na^+ into Contributions from Docking of Helical Strands, Formation of Helical Strands, and Unfolding of Low-Temperature Hairpins at Three Representative Temperatures

process		enthalpy changes (kcal mol^{-1}) 283 K	313 K	339 K
observed duplex formation	ΔH^o_{obs}	-61 ± 2	-98 ± 4	-120 ± 5
docking helical strands	ΔH^o_{dock}	-64 ± 3	-64 ± 4	-60 ± 6
residual single helix formation	$(13)(1 - \theta^{sh}_{S1})(\Delta h^{vH}_{shf,S1})$	-8 ± 1	-19 ± 2	-30 ± 3
	$(13)(1 - \theta^{sh}_{S2})(\Delta h^{vH}_{shf,S2})$	-9 ± 1	-20 ± 2	-30 ± 3
residual unfolding	$(\theta^{fold}_{S1})(\Delta H^o_{unfold,S1})$	13 ± 1	4 ± 1	0
	$(\theta^{fold}_{S2})(\Delta H^o_{unfold,S2})$	7 ± 1	1 ± 1	0

single strands is less ordered. At 313 K, this requirement for single helix formation (process II) prior to docking makes a very significant contribution (~40%) to the observed enthalpy of duplex formation. At 339 K, the enthalpic contributions of single helix formation are as large in magnitude as the contribution of docking to the observed $\Delta H°$.

Temperature dependences of the enthalpies of unfolding and of single helix formation estimated from differences in enthalpy contributions ($\Delta\Delta H°$) at the different temperatures listed in Table 6 clearly illustrate the origin of the large negative $\Delta C°_{obs}$ of DNA double helix formation detected by DSC and ITC. Enthalpically significant changes in the extent of folding and ordering of the unpaired strands in the temperature range of the ITC experiments (283−313 K) give rise to apparent heat capacity contributions of approximately −0.5 and −0.7 kcal K^{-1} (mol of duplex)$^{-1}$, respectively. In this range, $\Delta C°_{obs} = -1.3$ kcal K^{-1} (mol of duplex)$^{-1}$. In the temperature range which bridges the ITC and DSC experiments (40−65 °C), the corresponding apparent heat capacity contributions from unfolding and ordering are approximately −0.2 and −0.8 kcal K^{-1} (mol of duplex)$^{-1}$, respectively. In this range, the experimental value of $\Delta C°_{obs}$ is between −1.3 and −0.8 kcal K^{-1} (mol of duplex)$^{-1}$.

Previous ITC studies of duplex formation of oligomeric DNA sequences done in the context of thermodynamically dissecting the stability of more complex DNA structures such as triplexes (*9*) and Holliday junctions (*10*) also revealed large negative $\Delta C°_{obs}$ of duplex formation but were not interpreted quantitatively. An ITC study of interactions of single stranded polynucleotides with *E. coli* single stranded binding protein (SSB) by Ferrari and Lohman (*40*) showed that the origin of the large negative $\Delta C°_{obs}$ of complex formation between SSB and poly d[A] as compared to poly d[T] largely arose from changes in stacking in d[A] with temperature. We propose that the origin of $\Delta C°_{obs}$ reported in studies of DNA duplex formation also is from coupled equilibria in the strands, and that this phenomenon is likely a general feature of DNA duplex formation, not unique to poly[dA] or poly[A] sequences. Because the enthalpy of forming vertical base−base interactions (stacking) is large and noncooperative, any meaningful analysis of the stability of nucleic acid triplexes, quadruplexes, and junctions or other biologically relevant DNA or RNA structures should be referenced to a defined initial state (disordered or single helical) of the single strands.

ACKNOWLEDGMENT

We thank Dr. Oleg Tsodikov for helpful discussion and calculation of areas of overlap of adjacent bases in single helix formation and duplex formation, Dr. Craig Bingman for assistance in program development, and Drs. David Draper, Paul Hagerman, Michael Henzl, Eric Kool, Timothy Lohman, Julian Sturtevant, and Douglas Turner for valuable comments on the manuscript in advance of publication.

REFERENCES

1. Filimonov, V. V. (1986) in *Thermodynamic Data for Biochemistry and Biotechnology* (Hinz, H.-J., Ed.) pp 377−401, Springer-Verlag, Berlin.
2. Kool, E. T. (1997) *Chem. Rev. 97*, 1473−1487.
3. Turner, D. H. (1996) *Curr. Opin. Struct. Biol. 6*, 299−304.
4. SantaLucia, J., Jr. (1998) *Proc. Natl. Acad. Sci. U.S.A. 95*, 1460−1465.
5. Vesnaver, G., and Breslauer, K. J. (1991) *Proc. Natl. Acad. Sci. U.S.A. 88*, 3569−3573.
6. Shaio, D. D. F., and Sturtevant, J. M. (1973) *Biopolymers 12*, 1829−1836.
7. Nordmeier, E. (1992) *J. Phys. Chem. 96*, 1494−1501.
8. Korolev, N. I., Vlasov, A. P., and Kuznetsov, I. A. (1984) *Biopolymers 34*, 1275−1290.
9. Ladbury, J. E., Sturtevant, J. M., and Leontis, N. B. (1994) *Biochemistry 33*, 6828−6833.
10. Lu, M., Guo, Q., Marky, L. A., Seeman, N. C., and Kallenbach, N. R. (1992) *J. Mol. Biol. 223*, 781−789.
11. Filimonov, V., and Privalov, P. L. (1978) *J. Mol. Biol. 122*, 465−470.
12. Breslauer, K. J., Sturtevant, J. M., and Tinoco, I., Jr. (1975) *J. Mol. Biol. 99*, 549−565.
13. Freier, S. M., Sugimoto, N., Sinclair, A., Alkema, D., Neilson, T., Kierzek, R., Caruthers, M. H., and Turner, D. H. (1986) *Biochemistry 25*, 3214−3219.
14. Blake, R. D., and Delcourt, S. G. (1998) *Nucleic Acids Res. 26*, 3323−3332; erratum *Nucleic Acids Res. 27*, number 3 (1999).
15. Allawi, H. T., and SantaLucia, J., Jr. (1997) *Biochemistry 36*, 10581−10594.
16. Sugimoto, N., Nakano, S., Yoneyama, M., and Honda, K. (1996) *Nucleic Acids Res. 24*, 4501−4505.
17. Spolar, R. S., Ha, J.-H., and Record, M. T., Jr. (1989) *Proc. Natl. Acad. Sci. U.S.A. 86*, 8382−8385.
18. Privalov, P. L., and Gill, S. J. (1988) *Adv. Protein Chem. 39*, 191−234.
19. Spolar, R. S., Livingstone, J. R., and Record, M. T., Jr. (1992) *Biochemistry 31*, 3947−3955.
20. Spolar, R. S., and Record, M. T., Jr. (1994) *Science 263*, 777−784.
21. Murphy, K. P., and Freire, E. (1992) *Adv. Protein Chem. 43*, 313−361.
22. Privalov, P. L., and Makhatadze, G. I. (1992) *J. Mol. Biol. 224*, 715−723.
23. Makhatadze, G. I., and Privalov, P. L. (1995) *Adv. Protein Chem. 47*, 307−425.
24. Robertson, A. D., and Murphy, K. P. (1997) *Chem. Rev. 97*, 1251−1267.
25. Myers, J. K., Pace, C. N., and Scholtz, J. M. (1995) *Protein Sci. 4*, 2138−2148.
26. Laskowski, M., Sr. (1971) in *The Enzymes* (Boyer, P. D., Ed.) 3rd ed., Vol. 4, pp 313−328, Academic Press, New York.
27. Cantor, C. R., Warshaw, M. M., and Shapiro, H. (1970) *Biopolymers 9*, 1059−1077.
28. MicroCal, Inc. (1993) *Omega Ultrasensitive Isothermal Titration Calorimeter Instrument Instructions*, p 53, MicroCal, Inc., Northampton, MA.
29. Richmond, T. J. (1984) *J. Mol. Biol. 178*, 63−89.
30. Livingstone, J. R., Spolar, R. S., and Record, M. T., Jr. (1991) *Biochemistry 30*, 4237−4244.
31. Privalov, P. L., Ptitsyn, O. B., and Birshtein, T. M. (1969) *Biopolymers 8*, 559−571.
32. Frank-Kamenetskii, M. D., Anshelevich, V. V., and Lukashin, A. (1987) *U. Sov. Phys. Usp. 30*, 317−330.
33. Bond, J. P., Anderson, C. F., and Record, M. T., Jr. (1994) *Biophys. J. 67*, 825−836.
34. Leng, M., and Felsenfeld, G. (1966) *J. Mol. Biol. 15*, 455−466.
35. Epand, R. M., and Scheraga, H. A. (1967) *J. Am. Chem. Soc. 89*, 3888−3892.
36. Pörschke, D. (1976) *Biochemistry 15*, 1495−1499.
37. Hirao, I., Nishimura, Y., Tagawa, Y., Watanabe, K., and Miura K. (1992) *Nucleic Acids Res. 20*, 3891−3896.
38. Hirao, I., Kawai, G., Yoshizawa, S., Nishimura, Y., Ishido, Y., Watanabe, K., and Miura, K. (1994) *Nucleic Acids Res. 22*, 576−582.
39. Jollès, B., Réfrégiers, M., and Laigle, A. (1997) *Nucleic Acids Res. 25*, 4608−4613.

40. Ferrari, M. E., and Lohman, T. M. (1994) *Biochemistry 33*, 12896−12910.
41. Freier, S. M., Hill, K. O., Dewey, T. G., Marky, L. A., Breslauer, K. J., and Turner, D. H. (1981) *Biochemistry 20*, 1419−1426.
42. Dewey, T. G., and Turner, D. H. (1979) *Biochemistry 18*, 5757−5761.
43. Breslauer, K. J., and Sturtevant, J. M. (1977) *Biophys. Chem. 7*, 205−209.
44. Brahms, J., Michelson, A. M., and Van Holde, K. E. (1966) *J. Mol. Biol. 15*, 467−488.
45. Van Holde, K. E., Brahms, J., and Michelson, A. M. (1965) *J. Mol. Biol. 15*, 726−739.
46. Applequist, J., and Damle, V. (1966) *J. Am. Chem. Soc. 88*, 3895−3900.

BI990043W